JTTEE 2:271-282

Effect of Plasma Spray Processing Variations on Particle Melting and Splat Spreading of Hydroxylapatite and Alumina

S.J. Yankee and B.J. Pletka

Splats of hydroxylapatite (HA) and alumina were obtained via plasma spraying using systematically varied combinations of plasma velocity and temperature, which were achieved by altering the primary plasma gas flow rate and plasma gas composition. Particle size was also varied in the case of alumina. Splat spreading was quantified via computer-aided image analysis as a function of processing variations. A comparison of the predicted splat dimensions from a model developed by Madejski with experimental observations of HA and alumina splats was performed. The model tended to underestimate the HA splat sizes, suggesting that evaporation of smaller particles occurred under the chosen experimental conditions, and to overestimate the observed alumina splat dimensions. Based on this latter result and on the surface appearance of the substrates, incomplete melting appeared to take place in all but the smaller alumina particles. Analysis of the spreading data as a function of the processing variations indicated that the particle size as well as the plasma temperature and velocity influenced the extent of particle melting. Based on these data and other considerations, a physical model was developed that described the degree of particle melting in terms of material and processing parameters. The physical model correctly predicted the relative splat spreading behavior of HA and alumina, assuming that spreading was directly linked to the extent of particle melting.

1. Introduction

THE production of plasma-sprayed coatings requires the introduction of powdered materials into the plasma flame, where particles melt and attain sufficient momentum to impact the substrate to be coated. Droplets or splats spread outward on impact, solidify, and accumulate over time to form an aggregate coating. A critical aspect of the process is the extent of particle melting in the plasma flame for a given set of processing conditions. For example, if a particle becomes only partially molten on traveling through the plasma, it does not flatten and spread out on impacting the substrate, leading to a porous coating. On the other hand, if particles are exposed to an intensive thermal environment (high temperatures and long residence times in the plasma), some evaporation of the particles occurs, reducing the number and size of the particles striking the substrate and producing areas with sponge-like microporosity. Thus, obtaining a coating with desired characteristics in an economical fashion requires control of particle melting.

The purpose of the present article, therefore, was to examine how processing conditions affect particle melting by studying the influence of several process parameters on splat spreading. Earlier studies have shown the importance of particle size, temperature, and velocity at the time of impact on coating microstructure,[1] although parameters such as the droplet/substrate heat transfer characteristics could also be important. Because the coating microstructure is controlled by the particle characteristics on impact, these same parameters must also influence particle melting. Consequently, the present work has utilized not only variations in particle size, but also controlled variations in the primary plasma gas flow rate (PGFR) and the percent secondary gas (% secondary) to systematically examine the effects of these parameters on particle melting and subsequent splat spreading. This approach was adopted because the PGFR and % secondary, although having synergistic effects, influence the plasma velocity and enthalpy, respectively.

Key Words: alumina, cooling behavior, degree of melting parameter, hydroxylapatite, microstructure, modeling, splat deformation

S.J. Yankee and **B.J. Pletka,** Dept. of Metallurgical and Materials Engineering, Michigan Technological University, Houghton, MI 49931.

Nomenclature

A_n	Nozzle cross-sectional area (m^2)
d	Particle size (m)
E_k, E_s, E_v	Kinetic, surface, and viscous energies (J)
H	Plasma gas enthalpy (J/mole)
ΔH_m	Latent heat of fusion (J/mole)
k	Thermal conductivity ($J\ s^{-1}\ m^{-1}\ K^{-1}$)
$\dot{M}_g$	Plasma gas mass flow rate (kg/hr)
MW	Molecular weight (g/mole)
Re	Dimensionless Reynolds number
t	Time (s)
T	Temperature (K)
V	Plasma gas velocity (m/s)
W	Electrical power input (J/s)
W_{loss}	Rate of heat loss to the torch cooling water (J/s)
We	Dimensionless Weber number
ξ	Dimensionless splat radius
ρ	Density (g/cm^3)
ρ_g	Average plasma gas density (g/cm^3)

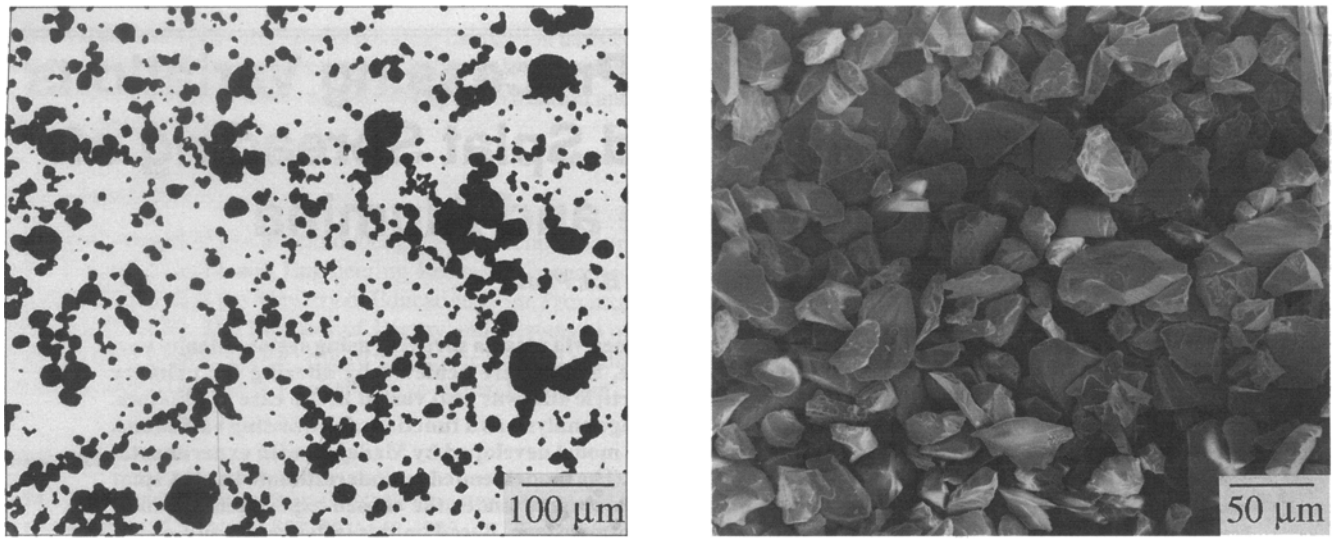

Fig. 1 (a) Transmitted light optical micrograph of air-classified HA powder showing spherical particles. (b) SEM micrograph of as-received Al_2O_3 powder, illustrating the angular nature of the particles.

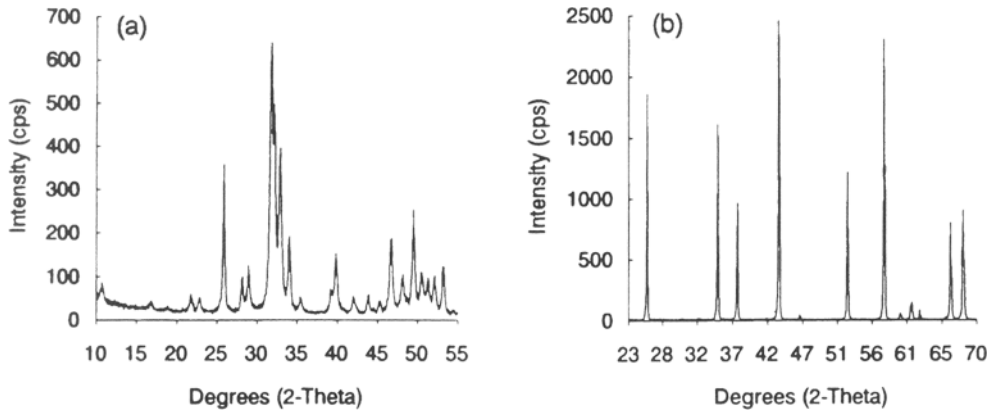

Fig. 2 X-ray diffraction scans of the as-received powder. (a) HA. (b) Al_2O_3.

Two ceramic materials, hydroxylapatite (HA)* and alumina (Al_2O_3), were used for the study. HA is a calcium phosphate material [$Ca_{10}(PO_4)_6(OH)_2$] frequently applied as a coating on biomedical orthopedic devices to aid implant fixation in the body. Alumina was chosen due to the wide variety of applications that use it as a coating for thermal and wear resistance. In addition, alumina serves as a model material because various material properties are available in the literature.

The study was conducted by examining the splats of each ceramic type/particle size combination after spraying at one of two selected levels for the PGFR and % secondary. This approach yielded four particle velocity/temperature combinations for each ceramic type/particle size. Computer-aided image analysis quantified the degree of splat spreading under each set of experimental conditions for both HA and Al_2O_3. Measurements of splat thickness were also performed. The extent of droplet spreading was analyzed using a model developed by Madejski[2] as a function of various processing conditions and material properties. This model was chosen because of its relative sim-

Table 1 Plasma spraying conditions

Parameter	HA	Alumina
Primary plasma gas	Argon	Argon
Secondary plasma gas	Helium	Helium
Carrier gas	Argon	Argon
Carrier gas flow rate, l/min	12.6	8.0
Powder flow rate, g/min	0.9	2.6
Amperage, A	1000	1000
Torch power, kW	40-50	38-45
Torch/substrate distance, cm	15.2	15.2
Chamber pressure, kPa	93	93
Chamber atmosphere	Argon	Air
Substrate material	Copper	Copper

*Equivalent terms that appear in the literature are hydroxyapatite and HAp.

Table 2 Experimental design for HA

Experiment No.	Primary gas flow rate, L/min		Percent secondary gas, vol%		Calculated velocity, m/s	Calculated temperature, K
1	High	57.0	Low	10	920	12,160
2	High	57.0	High	30	1030	13,760
3	Low	42.6	Low	10	710	12,480
4	Low	42.6	High	30	780	14,000

Table 3 Experimental design for alumina

Experiment No.	Primary gas flow rate, L/min		Percent secondary gas, vol%		Particle size, μm		Calculated velocity, m/s	Calculated temperature, K
1	High	49.6	High	30	High	33	940	14,480
2	High	49.6	High	30	Low	24	920	14,240
3	High	49.6	Low	0	High	33	770	11,680
4	High	49.6	Low	0	Low	24	800	12,000
5	Low	37.8	High	30	High	33	700	14,160
6	Low	37.8	High	30	Low	24	740	14,850
7	Low	37.8	Low	0	High	33	640	12,560
8	Low	37.8	Low	0	Low	24	610	12,000

plicity and its good agreement with more complex approaches such as that of Trapaga and Szekely.[3] It will be shown that the chosen processing conditions caused vaporization of HA particles, while a large fraction of the Al_2O_3 particles remained unmelted. Statistical analysis of the spreading data was performed and indicated the relative influence of each processing parameter on a given material system, including the potential importance of interactive effects between parameters. These results were used to develop a physical model to describe the degree of melting, and it will be shown that the model can correctly predict the relative spreading exhibited by the HA and Al_2O_3 splats.

2. Experimental Procedures

Nontransferred (DC) arc plasma spraying was carried out using a 120-kW system from Electro-Plasma, Inc., Irvine, CA, under the general conditions listed in Table 1. Hydroxylapatite powder was supplied by Monsanto Co., St. Louis, MO. The as-received powder was air classified to remove the ultra-fine particles, resulting in a size distribution of approximately 0.5 to 70 μm and a mean particle size of 8 μm. Traces of Ni and Fe were detected in the HA powder using a microprobe equipped with wavelength dispersive spectrometers, with the primary impurity being Mg (~0.6 at.%). Gray alumina was obtained from Metco Perkin-Elmer, Westbury, NY, as –325 mesh (<44 μm) powder. This powder was dry sieved to create two size fractions: –325 + 400 mesh (>37 μm) and –500 mesh (<25 μm). The corresponding particle sizes (equivalent spherical diameters) were determined by Microtrac (Leeds & Northrup, St. Petersburg, FL) analysis to be 33 and 24 μm, respectively. Chemical analysis results supplied by the manufacturer indicated 94.0% Al_2O_3, 2.5% TiO_2, 2.0% SiO_2, 1.0% Fe_2O_3, and 0.5% other oxides. Figures 1(a) and (b) are representative micrographs of the HA and Al_2O_3 powders, indicating the rounded morphology of the HA and the angularity of the alumina particles.

X-ray diffraction (XRD) scans of the as-received powders are shown in Fig. 2. Compared with JCPDS standards,[4] Fig. 2(a) indicates that only well crystallized HA was present in the powder. Figure 2(b) shows αAl_2O_3, with the exception of an additional peak at 2θ of about 62.3°. This phase could not be positively identified via comparison with JCPDS standards, although energy-dispersive spectrometry indicated the presence of isolated Ti-rich splats.

The experimental design employed for each material system is shown in Tables 2 and 3. Systematic changes in the chosen variables (PGFR; % secondary; and particle size, alumina) were made to examine the influence of each parameter on splat characteristics. Two values were selected for each parameter; these are designated as high and low in Tables 2 and 3.

Copper substrates of dimension 22 × 76 × 1.5 mm, having an average surface roughness of 0.1 μm, were cleaned with a 10% nitric acid solution and rinsed in distilled water. Copper was selected as a substrate material because an original (and uncompleted) goal of the work was to examine the influence of variations in substrate thermal conductivity on splat spreading. Splats were deposited on three coupons per each set of experimental conditions listed in Tables 2 and 3, using a single rapid pass of the torch perpendicular to the long dimension of the coupons.

Tables 2 and 3 also contain plasma temperatures and velocities calculated for each set of experimental conditions. The tabulated values apply to conditions at the nozzle exit and were calculated with the aid of the following equations. Equation 1 represents a simple energy balance at the nozzle exit and results in a calculation of the plasma enthalpy:[5]

$$W = W_{loss} + \dot{M}_g H \quad [1]$$

where W is the electrical power input; W_{loss} is the rate of heat loss to the torch cooling water; $\dot{M}_g$ is the plasma gas mass flow rate; and H is the plasma gas enthalpy at the nozzle exit. Corresponding plasma temperatures were then obtained from Fig. 1 in Ref 6. Plasma velocity at the nozzle exit was calculated from Eq 2:

$$V = \frac{\dot{M}_g}{\rho_g A_n} \quad [2]$$

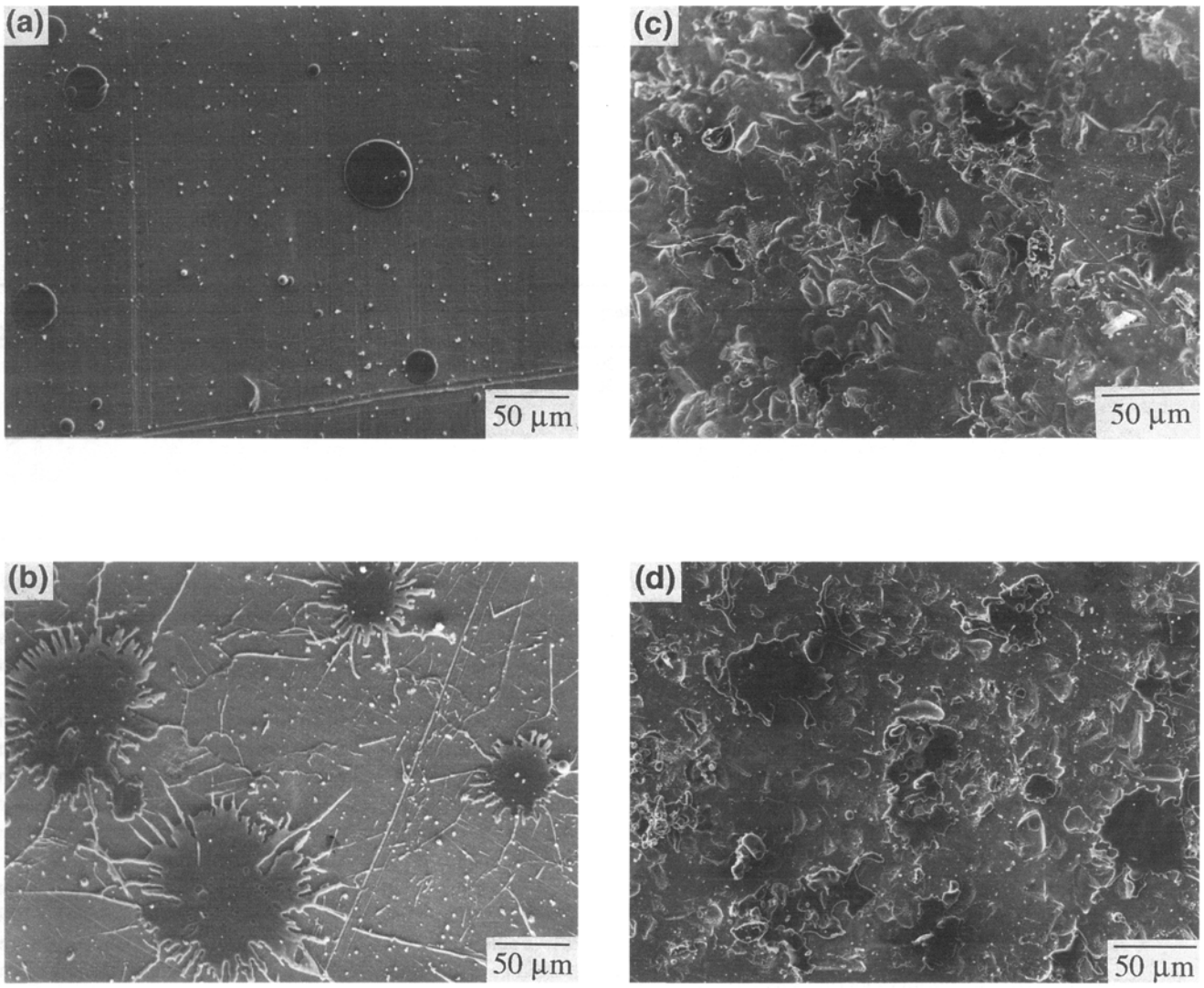

Fig. 3 SEM micrographs illustrating the types of splats produced by the experimental conditions listed in Tables 2 and 3. (a) HA, experiment 2. (b) HA, experiment 3. (c) Al_2O_3, experiment 4. (d) Al_2O_3, experiment 5.

where V is the plasma gas velocity at the nozzle exit, ρ_g is the average plasma gas density, and A_n is the nozzle cross-sectional area. The calculated values shown in Tables 2 and 3 indicate that the chosen PGFR and % secondary conditions were successful in achieving self-consistent variations in plasma velocity and temperature. The values found in Tables 2 and 3 do not represent measured characteristics of the droplets at impact; however, the droplet conditions are proportional to the calculated plasma temperatures and velocities[7] for a given particle size. Thus, relative comparisons assessing the effects of processing variations may be made between experiments.

One coupon was chosen randomly from each experiment and was carbon coated to examine the splats by scanning electron microscopy (SEM). Image analysis of isolated *in situ* splats was undertaken with the aid of a JEOL JXA-8600 microprobe (JEOL, Tokyo, Japan) equipped with a Link analysis system (Link Analytical, High Wycombe, England). Back-scattered electron images were used to obtain the greatest contrast for image analysis purposes. Uniformly spaced grids comprising at least 50 fields of view were established with automated stage control on the center of the spray pattern of each coupon studied. With this technique, at least 250 splat images were analyzed for each set of experimental conditions. Using the image analysis software, surface area measurements were obtained for the randomly selected splats; these data were converted to an equivalent circular radius, for which an average value was calculated for $\pm 3\sigma$ of the data population. These average dimensions were normalized with respect to the average starting particle radius, as determined via Microtrac analysis of the appropriate powder.

Splat thicknesses were measured with an optical microscope, using the sensitivity of the depth of field at high magnification. One coupon from each experiment was examined at a magnification of 1000×. The top surface of individual splats was brought into focus, followed by focusing on the surrounding substrate surface. Splat thickness in microns was measured by recording the respective readings on the calibrated scale of the

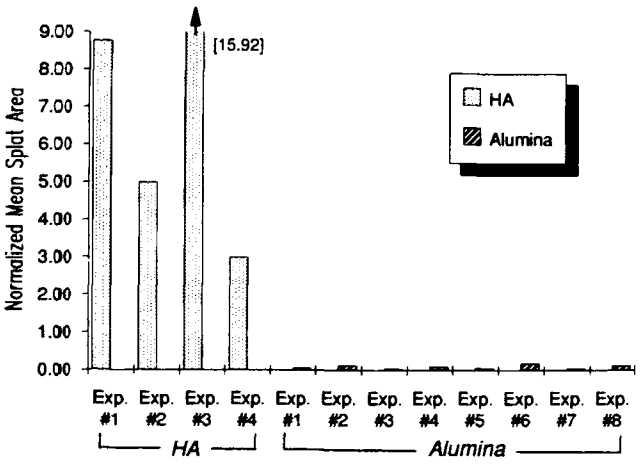

Fig. 4 Comparison of the mean splat areas determined from image analysis for each of the HA and Al_2O_3 experiments.

fine focus knob. To eliminate uncertainty due to mechanical slippage, focus was approached from the same direction for all measurements.

3. Results

Figure 3 consists of SEM micrographs illustrating the range of splat types obtained under the conditions listed in Tables 2 and 3 for the two material systems. Figures 3(a) and (b), from the HA experiments, show very circular and also extensively fingered splats, respectively. These two figures also indicate the differing sizes of the HA splats that formed. In contrast, the Al_2O_3 splats in Fig. 3(c) and (d) show less distinctive differences in morphology and overall smaller sizes. It may also be noted that the copper substrate has a different appearance in the HA and Al_2O_3 experiments; the substrate appears nominally smooth after spraying HA but pock-marked on spraying Al_2O_3. Because the pock-mark features resemble the alumina starting particle morphology, it was assumed that they represent the impact of unmelted particles during spraying.

Figure 4 illustrates the average splat area determined for each of the HA and Al_2O_3 experimental conditions; the data population analyzed was $\pm 3\sigma$ about the mean. The data were normalized by the surface area of the average starting particle size. It is apparent that, under the chosen conditions, HA splats attained much greater surface areas compared to Al_2O_3 splats. In addition, there was no substantial variation in spreading behavior of the alumina splats, although HA appears to be sensitive to variations in processing conditions. These image analysis results are consistent with the differing visual appearance of typical HA and Al_2O_3 splats, including the substrate appearance (Fig. 3). The observed splat behavior appears to be associated with differences in the degree of particle melting, which will be discussed in greater detail later.

As shown in Table 3, the alumina experimental design incorporated variations in mean particle size along with changes in PGFR and % secondary. The result was four sets of experiments in which all variables were held nominally constant except for particle size. Table 4 lists the particle size used for each experiment along with the average splat area found for each set of conditions. Comparing experiments 1 and 2, 3 and 4, etc., it may be noted that the smaller particle size consistently yielded the larger average splat area by an average of 23%. The improved spreading of the smaller particles was attributed to the fact that smaller volumes of material will heat faster. The surface area/volume ratio of the 24 μm particle size is ≈28% greater than that of the 33 μm particle size. Thus, these experiments indicate that a relatively small change in particle size affected splat spreading and illustrate the potential importance of particle size when optimizing plasma spraying conditions for a given material.

Table 4 Experimental splat area measurement for the various experiments

Experiment No.	Average particle size, μm	Splat area, μm^2	Normalized splat area
Al_2O_3			
1	33	187	0.05
2	24	221	0.12
3	33	139	0.04
4	24	186	0.10
5	33	240	0.07
6	24	317	0.18
7	33	159	0.05
8	24	224	0.12
HA			
1	8	1762	8.76
2	8	1006	5.00
3	8	3201	15.92
4	8	602	3.00

4. Discussion

Results from the current work indicate that there are distinct differences in the response of HA and Al_2O_3 to changes in the chosen processing conditions, although the range of calculated plasma/particle temperatures and velocities do overlap for the two systems (see Tables 2 and 3). For example, experiment 3 of HA and experiment 7 of alumina have similar calculated plasma temperatures, whereas the velocities are within ≈10%. Despite the approximately similar processing conditions, the degree of spreading exhibited by the splats in the respective experiments varied greatly. Because the average HA particle size was smaller by a factor of three or more compared to the average size of the Al_2O_3 particles, comparisons were made based on a parameter calculated by dividing the splat area by the surface area of the average sized original powder particle. All of these data are tabulated in Table 4. It can be seen that the normalized splat areas are much greater for the HA splats than for the Al_2O_3 splats.

Measured splat thicknesses indicated that only small variations existed between the various materials and processing conditions; mean HA splat thicknesses were 1.5 ± 0.6 μm for the four experiments and Al_2O_3 splat thicknesses were 1.9 ± 0.8 μm for the eight experiments. Because the alumina particles on average were larger than the HA particles and conservation of mass must be maintained, the approximate equality in splat thicknesses suggests that the smaller Al_2O_3 particles within the alumina particle size distribution were more easily melted and adhered to the substrate. Larger particles may not have melted

Table 5 Processing and material properties used in model calculations

Parameter	HA	Al_2O_3	Ref
Particle size, μm	8	24	...
Liquid surface tension, N/M	1.0	0.68	10
Liquid density, g/cm^3	2.52(a)	3.05	10
Spreading time, ms	1.0	1.0	11, 12
Torch-to-substrate distance, cm	15.2	15.2	...

(a) Estimated to be 80% of solid density

sufficiently to adhere and simply bounced off the substrate surface. This interpretation assumes that the impregnation of partially molten alumina particles in the soft copper substrate did not constitute a substantial fraction of the impact events. Examination of impacted alumina particles by SEM analysis indicated that relatively few partially melted particles appeared to be embedded to a substantial depth in the substrates. The differences in splat spreading between HA and Al_2O_3 may be attributed in part to heat transfer-related material properties. This topic will be discussed later in terms of the degree of melting of the two materials.

4.1 *Spreading of Hydroxylapatite: Model Versus Experiment*

Predictions of circular splat dimensions based on Madejski's model were compared with available experimental data for HA splats. Circular splats were not obtained in all of the HA experiments (Fig. 3), but the measured surface splat areas were converted to an equivalent circular radius to allow a comparison with Madejski's model. An analysis of the perturbations producing the "fingered" or "arm" morphology in Fig. 3(b) is deferred to a later publication.

The model developed by Madejski contains the following assumptions. Spreading is assumed to be complete prior to solidification of the liquid.[8] No splashing occurs (i.e., no material is lost), unlike the classic milk drop experiments of Worthington,[9] in which ligaments from edge perturbations become separated from the bulk of the impinging droplet. Laminar liquid flow, complete substrate wetting, and ideal heat transfer across the liquid/substrate interface are assumed. An incoming spherical liquid droplet attains the shape of a right circular cylinder of radius R_0 at impact with no energy losses, after which spreading occurs. This analysis neglects any shock/compressive effects at initial impact. The outer edge of the spreading liquid remains perpendicular to the plane of the droplet, and liquid thickness is dependent only on time.

The geometry of the model is shown in Fig. 5. The incoming droplet (Fig. 5a) of diameter D assumes the morphology shown in Fig. 5(b) at impact and spreads in the shape of a disk. The thickness, b, of the liquid splat is independent of spatial location and depends only on time (Fig. 5c).

The spreading of the liquid is assumed to fulfill the conservation of momentum described by the equation:[2]

$$\frac{dE_k}{dt} + \frac{dE_v}{dt} + \frac{dE_s}{dt} = 0 \qquad [3]$$

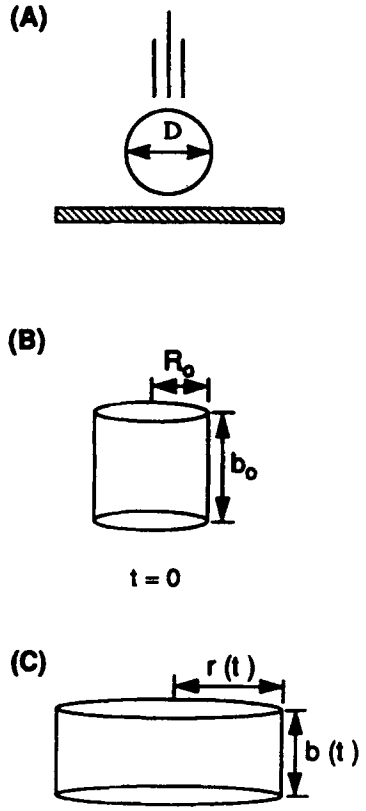

Fig. 5 Schematic of the assumed geometry used with Madejski's model. (a) A liquid droplet of diameter D impacts a rigid planar substrate, whereupon (b) the droplet assumes the form of a right circular cylinder of radius R_0 and height b_0 at impact after which the cylinder spreads (c) in a circular manner.

where E_k, E_v, and E_s are the kinetic, viscous, and surface energies, respectively; and t represents time. Physically, the kinetic energy attained by the particle as it passes through the plasma is dissipated by the rapid increase in friction or viscous energy as the splat spreads with a smaller contribution (dissipation) from increases in the total surface energy.[3] Substituting the appropriate expressions developed by Madejski for each term in Eq 3 results in the following second order, ordinary differential equation:

$$\frac{d}{dt}\left[\frac{\dot{\xi}^2}{18\varepsilon^2\xi^2}\left(\xi^2 + \frac{1}{30\varepsilon^6\xi^4}\right) + \frac{\xi}{We}\left(\xi + \frac{1}{3\varepsilon^3\xi^2}\right)\right] + \frac{6\varepsilon^3\xi^4\dot{\xi}^2}{Re} = 0 \qquad [4]$$

where ξ is the dimensionless splat radius (splat radius/original splat radius); ε is a constant equal to 0.5; We is the dimensionless Weber number; and Re is the dimensionless Reynolds number. The initial conditions for Eq 4 are:

$$\xi\,(\text{at } t = 0) = 1 \qquad [5]$$

and

Table 6 Calculated plasma conditions at nozzle exit and at impact, including experimental and theoretical values of ξ for HA and Al_2O_3

Experiment No.	Plasma velocity at nozzle, m/s	Plasma temperature at nozzle, K	Experimental ξ	Plasma velocity at impact, m/s	Plasma temperature at impact, K	Extrapolated liquid viscosity, poise	Theoretical ξ
HA-1	920	12,160	5.92	150	1460	0.83	2.65
HA-2	1030	13,760	4.47	170	1650	0.63	2.86
HA-3	710	12,480	7.96	120	1500	0.79	2.53
HA-4	780	14,000	3.46	130	1680	0.60	2.73
Al_2O_3-6	740	14,850	0.84	120	1780	0.92	3.22

Note: ξ is unitless.

$$\dot{\xi}(\text{at}\, t = 0) = \sqrt{\frac{3/2}{1 + 1/30\varepsilon^6}} \qquad [6]$$

The use of Madejski's model to calculate values of ξ required the processing and material parameters listed in Table 5. The remaining terms necessary for the model calculations, namely the particle impact velocity and liquid viscosity, were calculated in the following manner. The plasma velocity and temperature values in Table 2 were calculated at the torch nozzle exit; reductions in these conditions occur as the particles leave the torch nozzle until they strike the substrate. In-flight particle measurements by Vardelle *et al.*[1] of velocity and temperature as a function of distance along the axis of an Ar/H_2 plasma indicated on 83 and 88% drop, respectively, from the nozzle to a substrate positioned at a distance 15 cm away (the same distance used in the current work). Despite differences in the absolute value of the plasma conditions between the Vardelle study and the current work, the same relative decreases were applied to the nozzle temperature and velocity data listed in Table 2. This requires the assumption, however, that the velocity/temperature conditions imposed on the particles are identical to the plasma in which they travel. This assumption is supported by the fact that the measured velocities of particles, which had various sizes, have been found[1] to be in the range of 150 to 200 m/s at a torch-to-substrate distance of 15 cm, in reasonable agreement with the calculated range of 120 to 170 m/s of the present study. The total spreading time required as input for the calculations was maintained at 1×10^{-6} s for both HA and Al_2O_3.[11,12]

Having determined values of the particle temperature at impact for each experiment, these data were used to determine the viscosity of the liquid droplets at impact. Values for the liquid viscosity of calcium phosphates such as HA were unavailable; therefore, data for liquid alumina[10] at various temperatures were used. The available viscosity data were plotted versus homologous temperature, and a linear line of best-fit was determined. The curve was then used to estimate values of the liquid viscosity at impact (listed in Table 6) for each experiment from the homologous HA impact temperatures.

The splat sizes calculated using Madejski' s model (i.e., the theoretical ξ) are given in Table 6 and indicate that the model predictions underestimate the observed splat dimensions. The experimental value for the original splat radius was assumed to be equal to the average original particle radius. Although changes in the input parameters may improve the agreement between experimental and predicted values, another explanation is that evaporation of small particles within the particle size distribution took place in the plasma. This effect has the potential to effectively increase the average size of the remaining particles, resulting in larger splat sizes. If surface evaporation occurs, as was also observed by Das and Sivakumar[13] in their study of plasma sprayed alumina, it should take place in all particles, leading to a decrease in each individual particle size. However, smaller particles, which have a greater surface curvature and surface area to volume ratio than larger particles, should experience a greater rate of evaporation than the larger particles. The net result could be an average increase in size of the remaining particles. If this explanation is correct, it suggests that the chosen processing conditions subjected the HA particles to an intense thermal environment. Evidence in support of this suggestion will be presented later based on a physical model of particle melting.

4.2 *Spreading of Alumina: Model Versus Experiment*

A parallel study of model predictions was performed using available alumina splat spreading data obtained as a function of processing variations. However, the splats that resulted from the processing changes did not exhibit large differences in spreading behavior, which can be attributed to poor particle melting. Therefore, only the experiment producing the greatest average splat surface area was chosen for comparison with calculated spreading predictions, i.e., experiment 6. Converting the average measured splat surface area from this experiment to an equivalent circular radius yields a value of 10 μm, and normalizing by the starting particle size results in a measured ξ of 0.84.

The plasma conditions at the nozzle exit were calculated using the same approach as in the HA study and are listed in Table 6. The plasma/particle velocity and temperature at impact were calculated, including the particle liquid viscosity, using the technique described earlier. All other input parameters are listed in Table 5. From these data, a value for ξ of 3.22 was calculated using Madejski's model.

Several comments may be made about these calculations. An experimental value of ξ less than 1 is not physically possible unless the starting particle size was less than the measured value of 24 μm. Because the appearance of the substrates after spraying suggested that they were grit blasted by unmelted particles, the splats in Fig. 3(c) and (d) were probably formed by smaller particles in the size distribution that did melt in the plasma flame. Larger particles may have been only partially melted and/or unmelted and therefore did not adhere to the substrate. This inter-

Table 7 Analysis of variance results for splat spreading data

Parameter	Degrees of freedom	Variance	*F* statistic
HA			
Velocity	1	8.2E+05	7.4E+01
Temperature	1	6.1E+05	4.6E+01
Velocity × temperature	1	1.1E+06	1.0E+02
Error	552	1.1E+04	...
Alumina			
Velocity	1	2.2E+03	4.5E+00
Temperature	1	4.7E+04	9.8E+01
Particle size	1	2.1E−01	4.3E−04
Velocity × temperature	1	6.2E+03	1.3E+01
Velocity × size	1	1.9E+02	3.9E−01
Temperature × size	1	3.4E+04	7.0E+01
Velocity × temperature × size	1	1.8E+04	3.7E+01
Error	1629	4.8E+02	...

Note: *F* statistic at 99% confidence level = 6.66.

pretation also assumes that the particles did not substantially fragment in flight or on impact. Thus, the experimental processing conditions violated one of the assumptions of the model in that each powder particle was not necessarily fully molten at impact. As a result, Madejski's model overestimated the measured ξ values.

4.3 *Particle Melting*

A comparison of the experimental and predicted values of splat spreading has suggested that evaporation of HA particles took place during plasma processing, whereas many particles did not melt in the series of experiments conducted on Al_2O_3. The degree to which a liquid droplet spreads relative to the average starting particle size is directly related to the degree of particle melting, assuming viscous and surface tension forces may be overcome during spreading. Thus, the apparent inability of Madejski's model to predict the observed splat spreading of HA and Al_2O_3 stems from the fact that the model does not include heat transfer-related effects; that is, the actual degree of melting of the impacting particle is not modeled for a given set of plasma conditions. Modification of Madejski's model to incorporate such effects requires an understanding of the relevant material/processing parameters having a direct effect on spreading. The remainder of this article is devoted to identifying such parameters through an analysis of the HA and Al_2O_3 splat spreading data and to developing a physical model to describe the degree of melting based in part on this analysis, which combines material properties and processing conditions. The latter effort serves as a necessary precursor before trying to modify analyses such as those due to Madejski and yields a practical guide for estimating the "ease of melting" of a particular material for a given set of processing conditions.

The mean normalized splat area determined for each experiment was plotted against normalized velocity and temperature at the nozzle exit in Fig. 6(a) and (b). The velocities and temperatures were normalized to the lowest appropriate value calculated for each ceramic type. Figure 6(a) shows that the alumina splat spreading was essentially independent of plasma velocity,

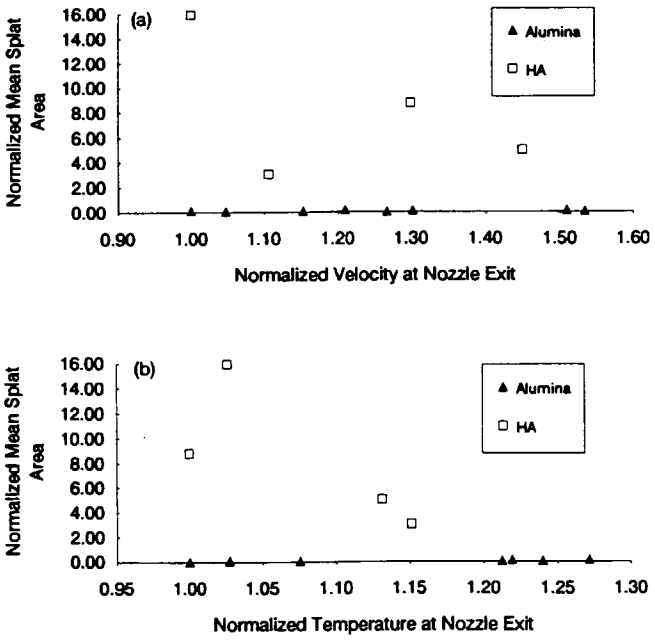

Fig. 6 Mean splat area for each experiment as a function of (a) normalized plasma velocity and (b) normalized plasma temperature at the nozzle exit.

whereas the HA data demonstrated a relatively strong inverse dependence over the range of velocities observed. The functional dependence of the HA data is believed to result from the shorter particle residence time in the plasma associated with increased velocities; i.e., shorter times in the plasma environment would allow less opportunity for heat absorption and hence a lesser degree of melting/splat spreading. The minimal sensitivity of Al_2O_3 to plasma velocity is attributed to the fact that alumina did not melt extensively under any of the chosen conditions.

A similar plot of normalized splat area versus the normalized calculated plasma temperature for each experiment is shown in Fig. 6(b). The HA data again show an inverse dependence, whereas on an expanded scale, the alumina data show a slight direct dependence over the range of temperatures studied. Splat area would be expected to increase as the temperature of the plasma increases (alumina data); however, the reverse relationship was found for the HA data. The significance of the HA data, because it violates what is believed to be the correct functional dependence, is not clear at this time.

Statistical analysis of the splat area data was also carried out to rank the relative influence of the chosen variables and to examine the interactions that may occur which affect the spreading data. This analysis was accomplished via standard two-way analysis of variance. Table 7 contains a summary of the analysis of variance for the splat size data ($\pm 2\sigma$ about the mean) for both the HA and Al_2O_3 systems. The *F* statistic is calculated based on the variance in the measured (image analysis) data, which may then be compared to values found in standard references for various confidence levels. When the calculated *F* is greater than the tabulated value, that parameter (temperature, velocity, or particle size) or the interaction of two or more parameters is considered significant in influencing the measured data. The *magni-*

Table 8 Calculated difficulty of melting factors for selected materials

Parameter	HA	Al_2O_3	ZrO_2	Fe
Solid density, g/cm^3	3.15	3.97	5.56	7.87
Heat of fusion, kJ/mole(a)	15.5	452.9	319.3	53.6
DMF	8.7	227.3	135.4	19.1

(a) Value listed for HA corresponds to tricalcium phosphate, a closely related compound. From JANAF data.

Table 9 Calculated DoM parameters and measured splat area

Experiment No.	DoM	Normalized splat area	Ratio of area/DoM
Alumina			
1	0.0038	0.05	13.2
2	0.0053	0.12	22.6
3	0.0037	0.04	10.8
4	0.0051	0.10	19.6
5	0.0050	0.07	14.0
6	0.0068	0.18	26.5
7	0.0049	0.05	10.2
8	0.0067	0.12	17.9
HA			
1	0.24	8.76	36.9
2	0.24	5.00	20.7
3	0.32	15.92	50.2
4	0.32	3.00	9.3

tude of the *F* statistic is indicative of the *degree* of influence of that parameter or interaction on the data.

Table 7 indicates that both velocity and temperature, along with their interaction, were found to be significant parameters at the 99% confidence level (see bottom of Table 7). HA splat spreading was influenced by all three parameters, but most strongly by the interaction of temperature and velocity in the processing range studied. In contrast, measured Al_2O_3 droplet spreading was most strongly affected by plasma temperature, followed by three of the four interaction terms. It may be noted that the statistically significant interactive effects each involved temperature.

It is difficult to compare the statistical analysis results between the two materials due to the relatively poor melting of the alumina. HA appeared to be "well melted," and the statistical analysis results may be accepted with confidence, unlike the case of Al_2O_3 where further experimentation to confirm the present results must be performed under more ideal melting conditions. In addition, although the influence of Al_2O_3 particle size was identified using mean values of splat area, the analysis of variance did not indicate the statistical significance of this parameter. The inability of the statistical analysis to confirm the influence of particle size on spreading is probably due to the small difference in particle sizes and the large scatter present in the data.

4.4 *Models for Particle Melting*

The ease of particle melting is not described by the melting temperature alone, but also by such material properties as the latent heat of fusion, ΔH_m, and the density of the material. Density influences particle trajectory through the plasma, whereas ΔH_m controls the solid to liquid transformation at the melting temperature. A "difficulty of melting factor" (DMF), shown in Eq 7, has been defined[14] to quantitatively rank the "meltability" of materials on the basis of these two material physical properties.

$$\text{DMF} = \frac{\Delta H_m}{\sqrt{\rho}} \qquad [7]$$

where ρ is the density. The calculated DMF values for HA and alumina are listed in Table 8, along with values for ZrO_2 and Fe, which are a commonly plasma-sprayed ceramic and metal, respectively. The data indicate that HA may be melted with relative ease compared to other ceramics and in fact has a DMF similar to that of iron. The calculated difference in the difficulty of melting between HA and Al_2O_3 is consistent with the magnitudes of the experimentally observed splat surface areas, suggesting the importance of ΔH_m, in particular, as a key determinant of melting success.

A term such as the DMF is very useful for rapid assessment of the relative spraying conditions necessary to melt given materials of a particular particle size. However, the present data, in addition to other investigations,[1] indicate that the particular plasma conditions through which a particle passes will also determine the degree of melting, in addition to heat transfer-related material properties. To incorporate the influence of both plasma and material properties, a physical model was developed to describe the degree of melting a particle achieves. Because the first step in building a mathematical model of a physical phenomenon is to identify all the parameters that may influence the phenomenon, the following analysis will attempt to identify those parameters that influence the degree of melting of particles in the plasma and to develop a dimensionless parameter that can describe this process.

The melting of a particle depends on plasma temperature and velocity. As discussed earlier, the residence time of a particle decreases as the plasma velocity increases, and greater particle melting should be achieved as the plasma temperature increases. Hence, the degree of melting (DoM) should depend on these parameters as:

$$\text{DoM} \propto \frac{T}{V} \qquad [8]$$

where T is the plasma temperature (K), and V is the plasma velocity (m/s). The material properties that should be important are thermal conductivity (k) and the enthalpy of fusion (ΔH_m). The former is important because, for a given particle size, the heat transferred into a solid depends directly on the thermal conductivity, whereas the latter controls the ease with which the solid to liquid transition is made. That is, as the enthalpy of fusion in-

Table 10 Material properties used for degree of melting calculations

Property	HA	Alumina
Mean particle size, μm	8	24 or 33
Solid density, g/cm^3	3.15	3.97
ΔH of fusion, kJ/mole	15.5	113.0
Molecular weight, g/mole	502.32	101.96
Thermal conductivity, J/m · s · K(a)	13.8	36.0

(a) Value for HA taken from values for fluorapatite and chlorapatite.[15]

creases in magnitude, melting becomes more difficult and the degree of melting should vary inversely with this term. The parameter becomes:

$$\text{DoM} \propto \frac{T \cdot k}{V \cdot \Delta H_m} \quad [9]$$

where k and ΔH_m have units of J s^{-1} m^{-1} K^{-1} and J/mole, respectively. As discussed earlier with regard to Eq 7, the density ($\rho \equiv$ g/cm^3) of a material influences the particle trajectory through the plasma and so varies inversely with the degree of melting parameter. The final material property that influences the degree of melting, as identified in other studies[1] and the current work, is the particle size (d). As the particle size decreases, the surface area to volume ratio increases, allowing more efficient heat transfer for a given thermal conductivity; therefore, the parameter varies inversely with particle size, which has units of length (m). To achieve a dimensionless parameter, the molecular weight (MW), which has units of g/mole, must be included, yielding

$$\text{DoM} = C\frac{T \cdot k \cdot \text{MW}}{V \cdot d \cdot \rho \cdot \Delta H_m} \quad [10]$$

where C is a constant of proportionality.

The degree of melting observed experimentally is related directly to the measured surface area of the impacted droplets. That is, more surface area from a given starting particle size corresponds to a greater degree of melting due to lower liquid viscosity. The normalized splat areas measured via image analysis may be compared to the DoM parameter calculated for each set of experimental conditions, which are tabulated in Table 9. Additional physical properties necessary for the calculations are listed in Table 10. Although the actual magnitudes of the DoM parameter calculations do not represent a physical quantity, the relative change in the parameter between HA and Al_2O_3 reflects the experimentally observed increase in HA droplet spreading. Thus, the physical model in Eq 10 appears to accurately reflect the relative degree of melting experienced by particles of various materials under a given set of processing conditions. It seems plausible that the insensitivity of Al_2O_3 splat spreading to processing variations (see Fig. 4) is due to the particles being insufficiently molten to exhibit significantly low values of liquid viscosity.

The data in Table 9 may be used to provide an additional qualitative measure of the validity of the DoM parameter. The DoM and the normalized splat area provide theoretical and experimental estimates, respectively, of the ease with which a particle of a given material may be melted. The ratio of these parameters (splat area/DoM) would be expected to be approximately constant, because a direct relationship exists between them, i.e., the more difficult it is to melt a material (smaller DoM) would result in less spreading (smaller area). The calculated ratios are shown in Table 9 and range in magnitude from ≈10 to 50. Considering that the data in the first two columns of Table 9 extend over two orders of magnitude, a factor of five difference in the ratios is considered reasonable. Thus, an internal check using the spreading data supports the validity of the physical model represented by the DoM parameter.

4.5 *Comparison with Related Studies*

Other studies of splat characteristics as a function of processing conditions may be found in the literature.[1,16,17] In general, these studies have qualitatively examined the effects of spray distance, particle size, and torch power on splat morphology. Fauchais and Houben have also reported on splat spreading relative to the initial powder particle size. Although systematic changes in powder or processing conditions were not made in these studies, the results indicate that conditions leading to greater thermal exposure of particles in the plasma flame tend to produce, as expected, more complete melting, and this was confirmed in the current work.

5. Summary

HA and Al_2O_3 splats were produced using systematic changes in the plasma velocity and temperature via systematic changes in the primary plasma gas flow rate and percent secondary gas. Despite having a smaller mean particle size, HA splats consistently possessed larger surface areas as determined via computer-aided image analysis, even when produced under approximately similar processing conditions as Al_2O_3. Underestimates of the experimental HA splat spreading data were obtained with Madejski's model, suggesting that evaporation of a portion of the smaller HA particle size distribution had taken place. In contrast, the Al_2O_3 splat dimensions predicted by Madejski's model overestimated the measured values. This result was attributed to melting only of smaller particles in the size distribution and/or to partial melting of larger particles. A statistical analysis of the splat data indicated that both plasma temperature and velocity as well as their interaction had an influence on the HA splat sizes. Alumina splat spreading was also found to be influenced by a number of synergistic effects; all of these involved temperature, which was the parameter of primary influence, although in general, poor Al_2O_3 melting was obtained under the chosen processing conditions.

A comparison of the HA and Al_2O_3 spreading data was made on the basis of the differences in material properties; the greater degree of HA droplet spreading was related to a previously proposed difficulty of melting factor which involved ΔH_m and density. A physical model based on plasma conditions and material properties was developed by identifying the variables that influence the degree to which particles melt in the plasma. Based on this approach, a dimensionless degree of melting parameter was derived and found to reflect the relative difference in droplet spreading of the two materials. This parameter may also serve as

a useful guide in selecting processing conditions for a given set of material properties that will lead to adequate melting of a given powder in the plasma spraying process.

Acknowledgments

The authors wish to thank Mr. W. Yates, Mr. E. Laitila, and Mr. L. Sutter for assistance with various aspects of this project. SJY received financial support from the Graduate School and from the Department of Metallurgical and Materials Engineering at Michigan Technological University. The project was partially funded by the Institute of Materials Processing at MTU.

References

1. M. Vardelle, A. Vardelle, P. Fauchais, and M. I. Boulos, Plasma-Particle Momentum and Heat Transfer: Modeling and Measurements, *AIChE J.*, Vol 29 (No. 2), 1983, p 236-243
2. J. Madejski, Solidification of Droplets on a Cold Surface, *Int. J. Heat Mass Transfer*, Vol 19, 1976, p 1009-1013
3. G. Trapaga and J. Szekely, Mathematical Modelling of the Isothermal Impingement of Liquid Droplets in Spraying Processes, *Metall. Trans. B*, Vol 22 (No. 6), 1991, p 901-914
4. Joint Committee on Powder Diffraction Standards, Swarthmore, PA, File numbers 10-173 (α-Al_2O_3) and 9-432 (HA)
5. D. Apelian, M. Paliwal, R. W. Smith, and W. F. Schilling, Melting and Solidification in Plasma Spray Deposition—Phenomenological Review, *Int. Met. Rev.*, Vol 28 (No. 5), 1983, p 271-293
6. H. Herman, Plasma Spray Deposition Processes, *MRS Bull.*, Vol 13 (No. 12), 1988, p 60-67
7. D. Matejka and B. Benko, *Plasma Spraying of Metallic and Ceramic Materials*, John Wiley & Sons, 1989, p 32
8. H. Jones, Some Principles of Solidification at High Cooling Rates, *RSP Principles and Technologies*, R. Mehrabian, B.H. Kear, and M. Cohen, Ed., Claitor's Publishing, 1978, p 28-45
9. A. M. Worthington, On the Forms Assumed by Drops of Liquids Falling Vertically on a Horizontal Plate, *Proc. Roy. Soc. London (A), Vol 25*, 1876, p 261-271
10. R. McPherson, On the Formation of Thermally Sprayed Alumina Coatings, *J. Mater. Sci.*, Vol 15 (No. 12), 1980, p 3141-3149
11. E. Garrity, D. Wei, and D. Apelian, Modeling of the Spreading Kinetics During Droplet Consolidation Processing, *Modeling and Control of Casting and Welding Processes IV*, A.F. Giamei and G.J. Abbaschian, Ed., TMS, 1988, p 593-602
12. C. Moreau, P. Cielo, and M. Lamontange, Flattening and Solidification of Thermally Sprayed Particles, *Thermal Spray: International Advances in Coatings Technology*, C.C. Berndt, Ed., ASM International, 1992, p 761-766
13. D.K. Das and R. Sivakumar, Modelling of the Temperature and the Velocity of Ceramic Powder Particles in a Plasma Flame. I. Alumina, *Acta Metall. Mater.*, Vol 38 (No. 11), 1990, p 2187-2192
14. R. McPherson, The Relationship Between the Mechanism of Formation, Microstructure and Properties of Plasma-Sprayed Coatings, *Thin Solid Films*, Vol 83, 1981, p 297-310
15. *Physical Properties of Rocks*, Subvolume a of Vol 1, G. Angenheister, Ed., Springer-Verlag, Heidelberg, 1982, p 311
16. J.M. Houben, Remarks Concerning a Rational Plasma for Thermal Spraying, *General Aspects of Thermal Spraying*, Nederlands Instituut voor Lastechniek, The Hague, 1980, p 143-154
17. H.D. Steffens, B. Wielage, and J. Drozak, Interface Phenomena and Adhesion of Thermal-Sprayed Composites, *Materialwissenschaft Werkstofftechnik*, Vol 21 (No. 5), 1990, p 185-194, in German